

Tunable Sponge-Like Hierarchically Porous Hydrogels with Simultaneously Enhanced Diffusivity and Mechanical Properties

Yousif Alsaïd, Shuwang Wu, Dong Wu, Yingjie Du, Lingxia Shi, Roozbeh Khodambashi, Rossana Rico, Mutian Hua, Yichen Yan, Yusen Zhao, Daniel Aukes, and Ximin He*

Crosslinked polymers and gels are important in soft robotics, solar vapor generation, energy storage, drug delivery, catalysis, and biosensing. However, their attractive mass transport and volume-changing abilities are diffusion-limited, requiring miniaturization to avoid slow response. Typical approaches to improving diffusion in hydrogels sacrifice mechanical properties by increasing porosity or limit the total volumetric flux by directionally confining the pores. Despite tremendous efforts, simultaneous enhancement of diffusion and mechanical properties remains a long-standing challenge hindering broader practical applications of hydrogels. In this work, cononsolvency photopolymerization is developed as a universal approach to overcome this swelling–mechanical property trade-off. The as-synthesized poly(*N*-isopropylacrylamide) hydrogel, as an exemplary system, presents a unique open porous network with continuous microchannels, leading to record-high volumetric (de)swelling speeds, almost an order of magnitude higher than reported previously. This swelling enhancement comes with a simultaneous improvement in Young's modulus and toughness over conventional hydrogels fabricated in pure solvents. The resulting fast mass transport enables in-air operation of the hydrogel via rapid water replenishment and ultrafast actuation. The method is compatible with 3D printing. The generalizability is demonstrated by extending the technique to poly(*N*-tertbutylacrylamide-*co*-polyacrylamide) and polyacrylamide hydrogels, non-temperature-responsive polymer systems, validating the present hypothesis that cononsolvency is a generic phenomenon driven by competitive adsorption.

1. Introduction

Hydrogels, cross-linked polymer networks with a highly porous structure and large water content, promise extensive applications in soft robotics,^[1] solar vapor generation,^[2] energy storage,^[3] drug delivery,^[4] catalysis,^[5] and biosensing^[6] owing to their softness, simple and tunable synthesis, functionalization, and stimuli-responsiveness. Most practical hydrogel applications, however, are constrained by the notably slow diffusion through their pore structure.^[7] Devices relying on mass transfer at the pore-water interface, such as for energy storage and catalysis, or water transport through the pores, such as for soft robotics and solar vapor generators, experience significant diffusion limitations necessitating scale down to miniature prototypes to sustain the required volumetric flowrates.^[8,9] The response rate of smart hydrogels is inversely proportional to the square of the hydrogel's smallest dimension.^[10] The mass transport through porous media can be improved by understanding tortuosity, a measure of how easily molecules can travel without experiencing obstacles, which can be characterized by geometric, electrical, and diffusive properties.^[11] The diffusive tortuosity is defined as the length traveled

between two points, L , divided by the shortest straight-line path between those points, L_0 , squared (Equation (1)).

$$\tau = \left(\frac{L}{L_0}\right)^2 \quad (1)$$

Through Einstein's equation of Brownian motion^[12] and semi-empirical pore-structure equations,^[13] the effective diffusion coefficient through hydrogels, D_{eff} , can be expressed as a function of a structure factor, p , the porosity, ϕ , and bulk solution diffusion coefficient, D_0 (Equation (2), Supporting Information, Equations S1–S5, Supporting Information)

$$D_{\text{eff}} = \frac{D_0}{1 + p(1 - \phi)} \quad (2)$$

Y. Alsaïd, Dr. S. Wu, D. Wu, Y. Du, L. Shi, R. Rico, M. Hua, Y. Yan, Y. Zhao, Prof. X. He

Department of Materials Science and Engineering
University of California, Los Angeles
Los Angeles, CA 90 095, USA
E-mail: ximinhe@ucla.edu

R. Khodambashi, Prof. D. Aukes
The Polytechnic School
Fulton School of Engineering
Arizona State University
Mesa, AZ 85 212, USA

 The ORCID identification number(s) for the author(s) of this article can be found under <https://doi.org/10.1002/adma.202008235>.

DOI: 10.1002/adma.202008235

It can be seen from Equation (2) that controlling pore size and pore structure of the hydrogel can directly affect the swelling rate, enabling high levels of tunability essential for controlled drug release, soft robot actuation, and high-speed sensing. To date, most works that improve swelling ratio and swelling rate do so by increasing the porosity (ϕ), the total volume fraction of pores.^[14,15] Superporous hydrogels, which boast the highest porosities and swelling rates among hydrogels, have been fabricated using porosigen,^[16–18] phase separation,^[19,20] particle crosslinking,^[21] and gas-blowing^[22,23] techniques. The larger pore sizes effectively reduce the tortuosity of the hydrogel and facilitate faster and greater water transport through the polymer matrix. However, increasing ϕ to increase effective diffusion coefficient typically results in a compromise in mechanical properties such as Young's modulus and toughness.^[24] Hydrogels with overly high porosities usually lack the necessary rigidity for practical applications.

Reconfiguring the overall pore structure, which tunes structure factor p , presents an alternative approach for increasing the effective diffusion coefficient in hydrogels. To date, this has been achieved via directionally aligned pore channels with built-in structural anisotropy.^[25–28] Although limiting diffusion to fewer dimensions reduces the tortuosity, it also reduces the total volumetric flux through the hydrogel due to the confinement of transport: even with maximum diffusion coefficient, that is, $D_{\text{eff}} \approx D_0$, the overall swelling properties of the hydrogel are limited by the total flux of water in the x , y , and z directions.^[29] Larger volumetric flowrates are especially needed for large hydrogels in scalable industrial applications, rendering 1D and 2D confined flux suboptimal.

The optimal stimuli-responsive hydrogel for fast diffusion must maintain 3D transport while exhibiting few diffusion obstacles, with moderate porosity; an overly high porosity, although can decrease tortuosity, compromises mechanical properties such as modulus and toughness due to a low polymer content. Based on these criteria, the hydrogel must exhibit a large degree of pore interconnectivity, so that most transport paths can approach a straight line.

To our knowledge, there remains a need for a generalizable technique to fabricate hydrogels with simultaneously enhanced diffusivity and mechanical properties from a variety of polymer backbones. In a recent review, Liu et al. report “in order to widen the application range of nanocomposite smart hydrogels, further improvement should be sought in terms of responsiveness, including responsive rate and degree, as well as mechanical properties, including Young's modulus, toughness, breaking strength, breaking strain, and so on.”^[10] To address this need for simultaneous enhancement in swelling and mechanical properties, which inhibits hydrogels' practical use in large-scale manufacturing, we propose cononsolvency photopolymerization for fabricating sponge-like hierarchically mesoporous hydrogels with simultaneously enhanced swelling and mechanical properties.

The cononsolvency effect is a relatively rare and still controversial phenomenon where the solubility of a macromolecule decreases or even vanishes in a mixture of two good solvents. This phenomenon was first reported for cellulose acetate dissolved in a mixture of aniline and acetic acid^[30] and later studied for poly(*N*-isopropylacrylamide) (PNIPAM)^[31–33] and

other polymers dissolved in different solvent mixtures, such as poly(vinyl alcohol) in dimethyl sulfoxide (DMSO)–water mixtures.^[34] To date, the cononsolvency effect has been primarily utilized to study the fundamental coil–globule–coil transition in PNIPAM linear chains,^[35,36] microgels,^[37,38] and macrogels synthesized in pure solvents then immersed in mixed solvents.^[39] While some works have reported polymerization of hydrogels in different mixed solvent environments and observed changes in their properties,^[40,41] very few have generated hierarchically structured and highly-interconnected pores. Remarkably, Tokuyama et al. showed that a 24 h thermally initiated polymerization of PNIPAM in *N,N*-dimethylformamide (DMF)–water mixed solvent could produce structures with enhanced thermally responsive deswelling rate;^[42] however, the swelling rate, an equally important property, and mechanical characterizations were neglected. To date, no work systematically studies the effects of reaction parameters of cononsolvency polymerization, such as solvent composition and temperature, to develop a generalizable technique for producing hydrogels with simultaneously enhanced swelling and mechanical properties. Additionally, all these works employ 12–24 h thermally initiated reactions, incompatible with rapid manufacturing.

In this work, we have developed a general, facile, and rapid cononsolvency photopolymerization technique for various materials, using PNIPAM in DMSO–water conosolvent mixtures as an exemplary system, to synthesize hydrogels exhibiting twofold enhancements in swelling ratio and Young's modulus, and a sixfold enhancement in deswelling rate compared to a hydrogel control synthesized with a conventional pure solvent method. This technique takes advantage of simultaneous crosslinking and cononsolvency-induced polymer collapse to generate hierarchically structured and interconnected polymer networks. We have systematically investigated the effects of solvent composition and reaction temperature on the microstructures, mechanical properties, and swelling-deswelling performance of the resulting hydrogels. By leveraging the structure-property insights, we developed 3D-printable PNIPAM hydrogels with broadly tunable swelling and mechanical properties and also extended this principle to other polymer hydrogel systems.

PNIPAM is primarily investigated owing to its well-documented cononsolvency properties and widespread use as a stimuli-responsive material. With a lower critical solution temperature (LCST) of 31–34 °C, closely matching the human body temperature, PNIPAM is a highly promising candidate hydrogel for biomedical applications; when the temperature is below the LCST the hydrogel swells and becomes hydrophilic, and when it is above the LCST the hydrogel collapses and becomes hydrophobic.

2. Results and Discussion

PNIPAM hydrogels were synthesized via free-radical UV photopolymerization in different mixed solvent compositions, as shown schematically in Figure 1a. In pure solvent environments, the polymerization yields regular closed-cell pores, termed closed pores, while in specific mixed solvent conditions, the pores exhibit hierarchical open-celled pores, termed open

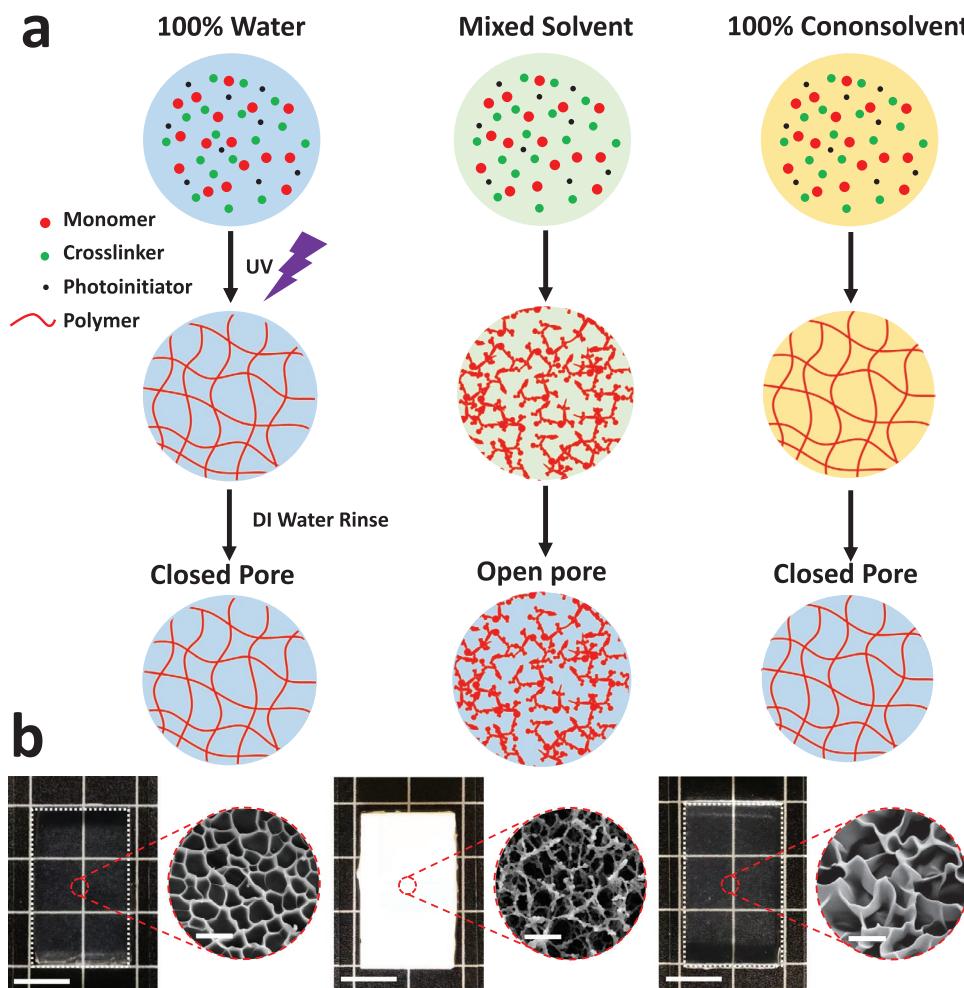


Figure 1. a) Schematic of the mixed solvent photopolymerization technique which utilizes the cononsolvency effect to generate hydrogels with hierarchically structured open pores. b) Optical photos (scale bar: 1 cm) and SEM images (scale bar: 5 μm) of PNIPAM hydrogels photopolymerized in 0 mol% (left), 40 mol% (middle), and 100 mol% (right) DMSO.

pores, with a high degree of interconnectivity caused by the simultaneous crosslinking and cononsolvency-induced collapse during photopolymerization. The pore structure and hydrogel properties can be tuned via careful selection of solvent composition and reaction temperature to achieve both enhanced swelling and mechanical performance. Figure 1b depicts photos and scanning electron microscopy (SEM) images of PNIPAM hydrogels photopolymerized in pure water, pure DMSO, and mixed DMSO–water solutions; it is readily observed that the hydrogels synthesized in the pure water and DMSO solvents were optically transparent, while the mixed solvent synthesized gel was white and opaque.

To better characterize the cononsolvency phenomenon, it is preferable to focus on polymer solutions rather than cross-linked polymer hydrogels; polymer solutions exhibit reversible coil-to-globule transitions which can be observed in real time, unlike cross-linked polymer hydrogels where the coils or globules are fixed due to crosslinking. The polymer structures that can be generated with cononsolvency photopolymerization require specific solvent systems and reaction conditions; not all mixed solvent systems exhibit the cononsolvency phenomenon with

the desired polymer backbone. In the case of linear PNIPAM chains, mixtures of water–DMSO,^[35] water–methanol,^[32,43] and water–ethanol^[44] have been extensively studied. Although it is possible to synthesize these hierarchical open pore PNIPAM hydrogels in any of these reported cononsolvent systems, we focus on the water–DMSO system for simplicity. PNIPAM chains exist in the coil state in pure water and pure DMSO solvents; they collapse into globules in DMSO–water mixtures (Figure 2a). Although the reason for this polymer collapse in specific mixed solvents is controversial, the most commonly accepted explanation is that it is a consequence of the generic competitive adsorption phenomenon;^[45] specifically, for PNIPAM in DMSO–water mixtures, DMSO behaves as a stronger solvent than water, so it competes for adsorption sites along the polymer backbone. When the boundary layer surface of the PNIPAM chains is saturated with DMSO, the entire polymer surface becomes more hydrophobic and rejects water, causing polymer coils to collapse into globules (Figure S1, Supporting Information), which scatter more light. The coil-to-globule transition can hence be tracked by observing the solution turbidity. At room temperature, the turbidities of

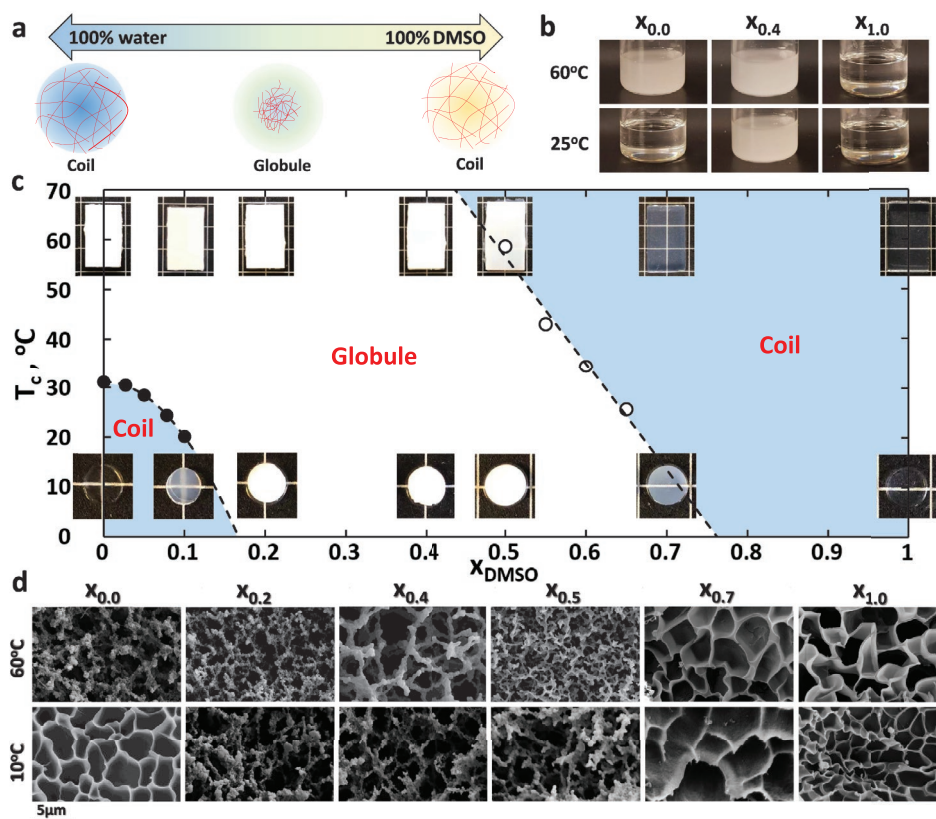


Figure 2. a) Schematic of the cononsolvency effect for PNIPAM polymer chains in mixtures of DMSO and water, demonstrating the coil–globule–coil transition behavior. b) Photos of UV-photopolymerized PNIPAM chains (non-crosslinked) dissolved in 0 mol% (left), 40 mol% (middle), and 100 mol% (right) DMSO solutions at 25 and 60 °C. c) Phase diagram showing the lower critical solution temperature (solid circles) and upper critical solution temperature (hollow circles) of PNIPAM chains dissolved in DMSO–water solutions with varying DMSO mole fractions, x_{DMSO} . Shaded and unshaded regions correspond to the conditions where PNIPAM exists in the coil and globule states, respectively. Inset photos show PNIPAM hydrogels synthesized at the corresponding temperatures and solvent compositions, with optical transparency consistent with the solution phase boundaries. d) SEM images of PNIPAM hydrogels synthesized at different x_{DMSO} and temperatures.

PNIPAM solutions in 0, 40, and 100 mol% DMSO (Figure 2b) correspond to the expected coil–globule–coil transition behavior described in Figure 2a; namely the polymer solutions are optically transparent in pure water and DMSO solvents, where coils are expected, but not in a DMSO–water mixture, where globules are expected. In comparison, above the LCST of ≈ 31 °C, PNIPAM dissolved in 0 mol% DMSO (100 mol% water) becomes turbid due to LCST-induced globule formation. For simplicity, a subscript notation is used to indicate the DMSO mole fraction of the solvent; for example, $x_{0.4}$ refers to a DMSO mole fraction, x_{DMSO} , of 0.4.

Since globules scatter more light than polymer coils, the coil-to-globule transition can be characterized by measuring the cloud-point temperature of the PNIPAM solutions at different x_{DMSO} (Figure S2, Supporting Information). These cloud-point temperatures of PNIPAM solutions define the boundaries of the phase diagram in Figure 2c. It is readily observed that the PNIPAM solutions experience LCST and upper critical solution temperature type behavior at low and high x_{DMSO} values, respectively. Overlaid on the phase diagram are photos of cross-linked PNIPAM hydrogels synthesized at 60 °C (rectangle-shaped) and 10 °C (circle-shaped). The optical transparencies of the hydrogel

samples are consistent with the phase diagram obtained from turbidity measurements of the non-crosslinked PNIPAM solutions. Specifically, hydrogels polymerized within the globule region exhibited high levels of scattering, resulting in an opaque white appearance, while those polymerized within the coil regions appeared optically transparent. Additionally, unlike in non-crosslinked PNIPAM solutions, the globules formed in the PNIPAM hydrogels were permanent due to chemical crosslinking. Hence, hydrogels polymerized within the globule region remained white, despite being immersed in 25 °C deionized (DI) water for 24 h post-synthesis; all the hydrogel images in Figure 2c were taken after complete rinsing in room temperature deionized water. We confirmed that the cononsolvency-induced opacity does not significantly affect the pore size homogeneity, nor does it significantly limit sample size from UV penetration issues, due to the fast photopolymerization reaction (Figure S3, Supporting Information). SEM images were taken of these crosslinked PNIPAM hydrogels synthesized with cononsolvency photopolymerization (Figure 2d) showing closed pore and open pore structures for hydrogels synthesized within the coil and globule regions, respectively. Fourier transform infrared (FTIR) spectroscopy was also performed on

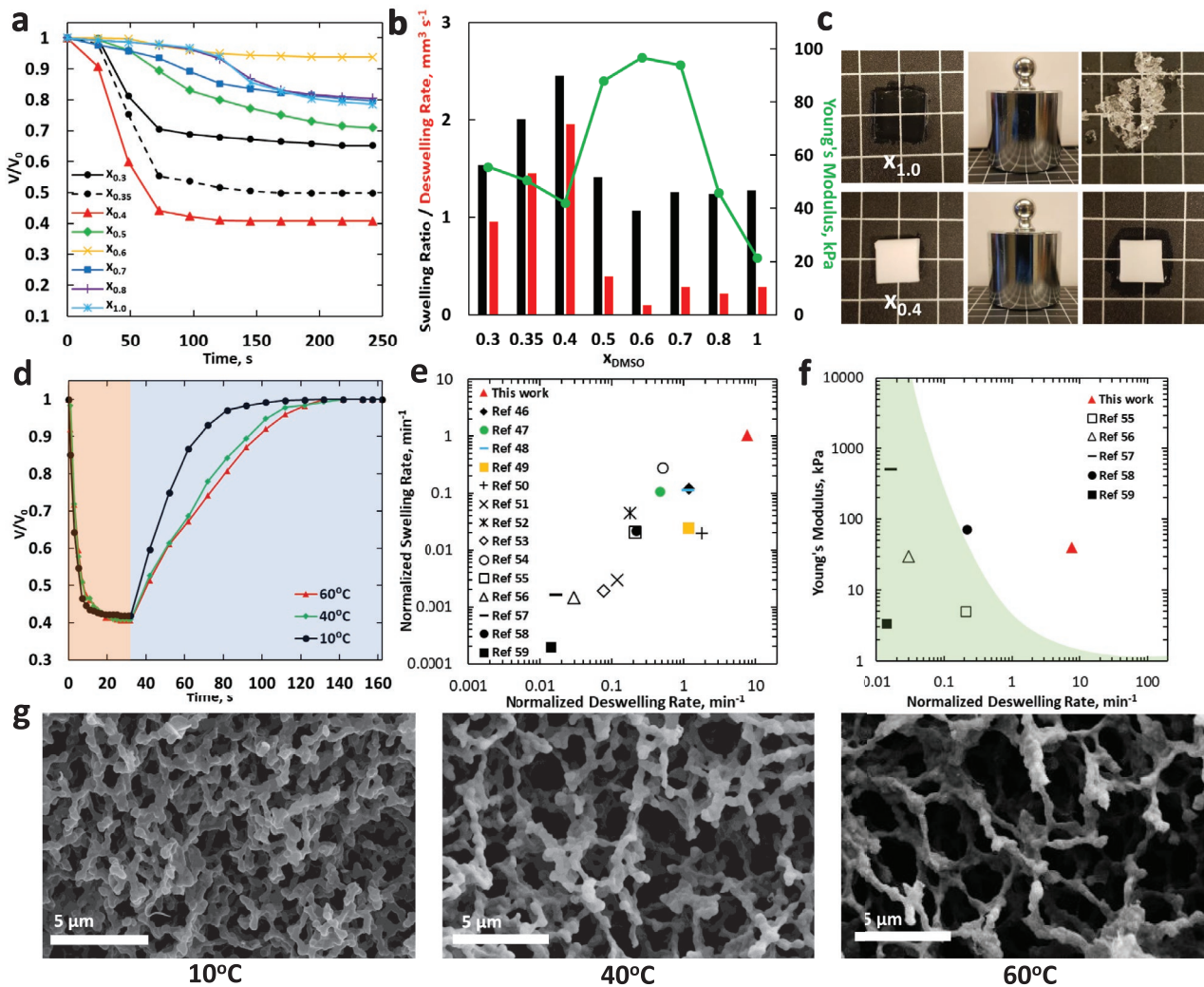


Figure 3. a) Deswelling curves for PNIPAM hydrogels (10 mm diameter, 3 mm thickness) photopolymerized in different DMSO mole fractions upon immersion in 60 °C DI water. b) Compiled swelling ratios, deswelling rates, and Young's moduli of the PNIPAM hydrogels. c) Compression test of $x_{1,0}$ (closed pore) and $x_{0,4}$ (open pore) hydrogel samples under 500 g load. d) Deswelling (60 °C, orange region) and swelling (25 °C, blue region) of $x_{0,4}$ gels polymerized at different temperatures. e) Comparison of volumetric swelling and deswelling rates with the reported literature on fast-responsive PNIPAM hydrogels, normalized by their respective swollen volumes. Normalization was performed by dividing the calculated volume change rate by the swollen hydrogel volume. (For refs. [48, 55, 57, and 58]: swelling rate was estimated to be 0.1 times the deswelling rate). f) Comparison of Young's modulus and normalized deswelling rate with the reported literature. (The Young's modulus in ref. [57] was measured in compression, while the others were measured in tension). g) SEM images of $x_{0,4}$ gels photopolymerized at 10 °C (left), 40 °C (middle), and 60 °C (right).

$x_{0,4}$ and $x_{1,0}$ hydrogels polymerized at 60 °C to confirm the two are chemically identical (Figure S4, Supporting Information).

It is found that a higher monomer wt% (Figure S5, Supporting Information) yielded superior swelling behavior and Young's modulus (Figure S6, Supporting Information). **Figure 3a** depicts the time-dependent deswelling behavior of PNIPAM hydrogels synthesized at 60 °C in different x_{DMSO} environments; the $x_{0,4}$ sample exhibited the highest swelling ratio and deswelling rate. This is consistent with the SEM image of $x_{0,4}$ (Figure 2c) depicting an open pore structure with large and highly interconnected pores compared to gels synthesized at other x_{DMSO} conditions. In **Figure 3b**, Young's moduli were calculated from stress-strain measurements (Figure S7, Supporting Information) obtained with dynamic mechanical analysis (DMA) and overlaid on top of swelling ratio and deswelling rate extracted from

Figure 3a. Compared to the closed pore PNIPAM synthesized at $x_{1,0}$ (the control), the open pore PNIPAM synthesized at $x_{0,4}$ resulted in a twofold increase in swelling ratio and Young's modulus, and a sixfold increase in deswelling rate. A discontinuous increase in swelling ratio and deswelling rate is readily observed as DMSO mole fraction reduces from $x_{0,5}$ to $x_{0,4}$, despite gravimetric measurements indicating that water content of the final prepared hydrogels decreases gradually with decreased DMSO mol fraction (Figure S8, Supporting Information); this supports the idea that the diffusion enhancement comes primarily from the pore structure enabling faster 3D transport, rather than the porosity. Toughness was evaluated by placing a 500 g load on top of the $x_{1,0}$ and $x_{0,4}$ gels (Figure 3c); the $x_{1,0}$ hydrogel, with a typical closed pore structure, was destroyed while the $x_{0,4}$ hydrogel with open pore structure remained intact.

As described by the phase diagram in Figure 2c, the cononsolvency phenomenon is not only a function of solvent composition, but also a function of temperature. Hence, the effect of reaction temperature on hydrogel pore structure and performance was also investigated. The temperature of the $x_{0.4}$ prepolymer solutions was measured throughout the duration of the cononsolvency photopolymerization reaction under ambient conditions, active cooling, and pulsed illumination with active cooling (Figure S9, Supporting Information), corresponding to reaction temperatures of 60, 40, and 10 °C, respectively. The time-dependent deswelling and swelling of these $x_{0.4}$ PNIPAM hydrogels are measured upon sequential immersion into 60 and 25 °C baths, respectively (Figure 3d). It is readily observed that gels fabricated at all three reaction temperatures exhibited the same swelling ratio and deswelling performance, while the gel synthesized at 10 °C swelled the fastest. Based on the SEM images of these three hydrogels (Figure 3g), this enhanced transport can be attributed to the smaller, but still highly interconnected, pore structure of the 10 °C $x_{0.4}$ gel that results in higher capillary pressure. Normalized swelling and deswelling rates of the 10 °C sample were calculated by dividing the volume change rates obtained from Figure 3d by the swollen hydrogel volume, then compared to those calculated from some

representative literature focusing on fast stimuli-responsive PNIPAM hydrogels (Figure 3e).^[46–59] In this comparison, it is readily observed that both normalized swelling and deswelling rates in this work are about an order of magnitude higher than what has been reported. Comparing to the few works measuring both the deswelling rate and Young's modulus of their PNIPAM hydrogels, this work demonstrates a record-breaking order of magnitude improvement in both properties without compromise (Figure 3f).

One of the significant limitations of hydrogels is the requirement of submersion in water: due to severe transport limitations, hydrogels cannot be exposed to air for long durations because evaporation rates are generally higher than swelling rates, resulting in undesired deswelling and drying. We fabricated $x_{1.0}$ and $x_{0.4}$ PNIPAM hydrogel pillars and exposed them to air for 24 h to dry; remarkably, these pillars were able to support themselves upright in air due to their rigidity. Afterward, we added DI water to the base of the pillars and observed the swelling behaviors. The $x_{0.4}$ pillar was able to rehydrate itself in air completely within 60 min, while the $x_{1.0}$ pillar could not, no matter how long we waited (Figure 4a). This suggests that cononsolvency photopolymerization for fabricating spongy open pore hydrogels presents a promising

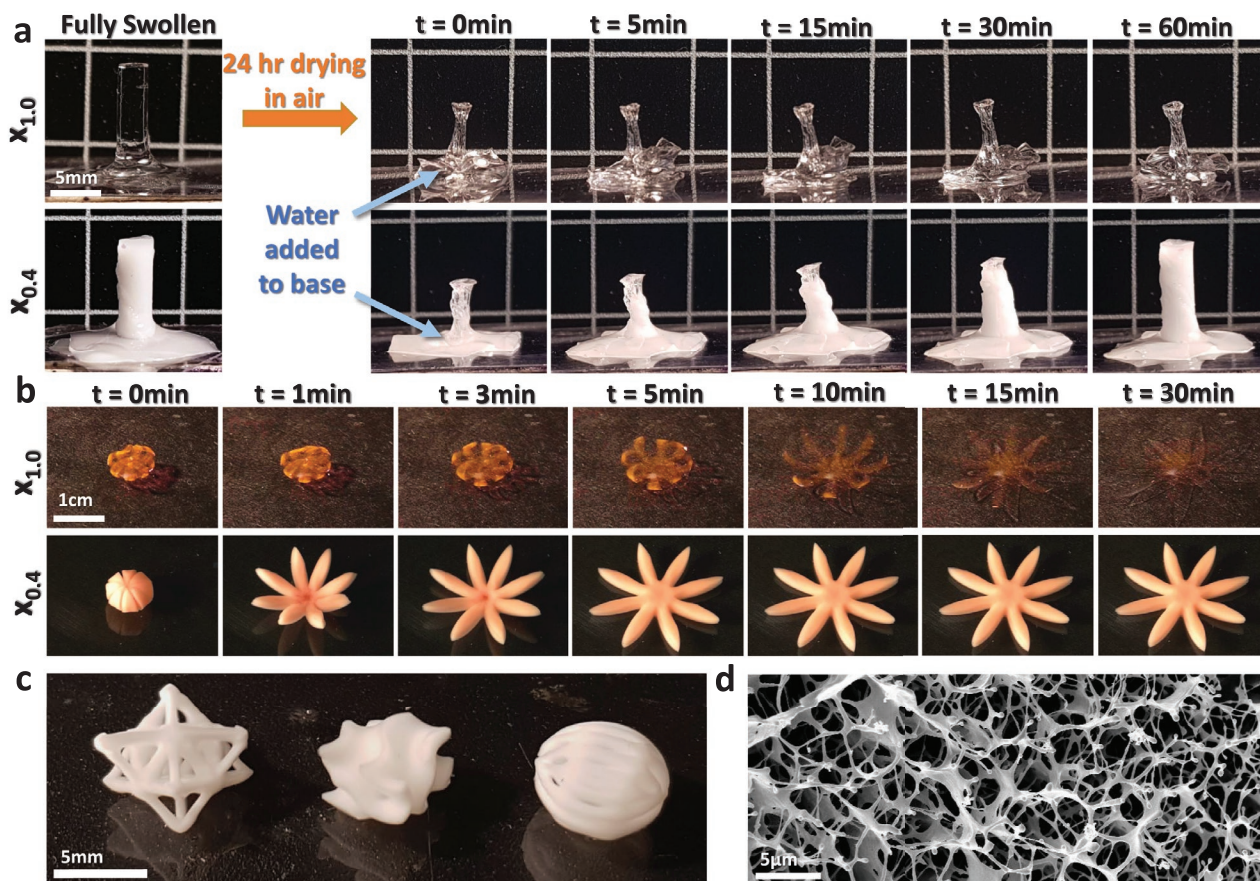


Figure 4. a) In-air swelling behaviors of $x_{1.0}$ and $x_{0.4}$ gel pillars, which were dried in air first and then supplied with water at the base. b) Swelling-induced blooming behaviors of 3D printed $x_{1.0}$ and $x_{0.4}$ gel flowers shrunken at 60 °C then immediately immersed in 25 °C water. c) 3D-printed octet-truss (left), gyroid (middle), and ovoid (right) structures from a modified $x_{0.4}$ PNIPAM precursor solution. d) SEM of the 3D-printed PNIPAM, confirming open-celled pore structure.

direction for in-air hydrogel applications, as long as there is a constant water supply. The cononsolvency photopolymerization technique is also compatible with 3D printing, as shown in Figure 4b where the swelling behaviors of printed $x_{1,0}$ and $x_{0,4}$ PNIPAM flower structures were characterized; these structures were printed using modified $x_{1,0}$ and $x_{0,4}$ precursors, described comprehensively in the Supporting Information. The flowers can be observed to bloom when immersed into a 25 °C water bath from 60 °C; Figure 4b depicts that the $x_{0,4}$ flower was able to fully bloom six times faster than the $x_{1,0}$ flower. To further showcase the 3D printability, we printed various other structures from the modified $x_{0,4}$ precursor (Figure 4c), and confirmed open-celled pore structure with SEM (Figure 4d).

Mukherji et al. suggested that polymer collapse in miscible good solvents is not specific to PNIPAM systems, rather it is generic.^[45] The work specifies that three criteria must be met to achieve cononsolvency-induced polymer collapse: the pure solvent and pure cosolvent must both be able to fully dissolve the polymer, the solvent and cosolvent must be mutually miscible, and the cosolvent must behave as a stronger solvent for the polymer than the solvent. After exploring the role of cononsolvency in fabricating open pore gels from PNIPAM, we extended the principle of cononsolvency photopolymerization to polyacrylamide (PAM) and poly(*N*-tertbutylacrylamide-*co*-polyacrylamide) (PNTBAM-*co*-PAM) hydrogel systems (Figure 5a) and fabricated similar open pore structures (Figure 5b). As expected, these hierarchically structured open pores resulted in a white opaque appearance, similar to what was observed in PNIPAM. It was observed that for PAM hydrogels, the closed pore and open pore structures occurred at $x_{0,0}$ and $x_{0,6}$ rather than the expected $x_{1,0}$ and $x_{0,4}$ DMSO mole fractions, respectively; in other words, the phase behavior is inverted. This is

likely due to the higher hydrophilicity of PAM, in which water acts as a stronger solvent than DMSO, in contrast to PNIPAM and PNTBAM-*co*-PAM systems; when the mole fraction is rewritten with respect to water instead of DMSO, one obtains the expected $x_{1,0}$ and $x_{0,4}$ for closed pore and open pore structures, respectively. To confirm enhanced diffusion resulting from the open pore structure, a capillary wicking experiment was used since PAM and PNTBAM-*co*-PAM do not demonstrate clear thermo-responsiveness (Figure 5c); a fresh tissue is applied to the surface of the hydrogels every minute to absorb water, and the mass loss is recorded (Figure 5d), confirming that for all three hydrogel systems, the opaque open porous polymer structure exhibited increased water loss due to capillary wicking.

3. Conclusion

In this work, we have developed cononsolvency photopolymerization as a general, tunable, scalable, and one-pot-compatible technique for synthesizing hierarchically structured open pore hydrogels with simultaneously enhanced swelling and mechanical properties, typically contradictory characteristics. PNIPAM as an exemplary material was systematically investigated and shown to exhibit a twofold enhancement in swelling ratio and Young's modulus and a sixfold enhancement in deswelling rate. The pore structure is tunable not only by controlling the solvent composition but also the reaction temperature. PNIPAM hydrogels synthesized with this method carry the potential for in-air applications, due to the ultrafast water transport. The method is compatible with 3D printing and has been generalized to other polymer systems. While simultaneous enhancement of diffusion and mechanical properties can greatly benefit porous

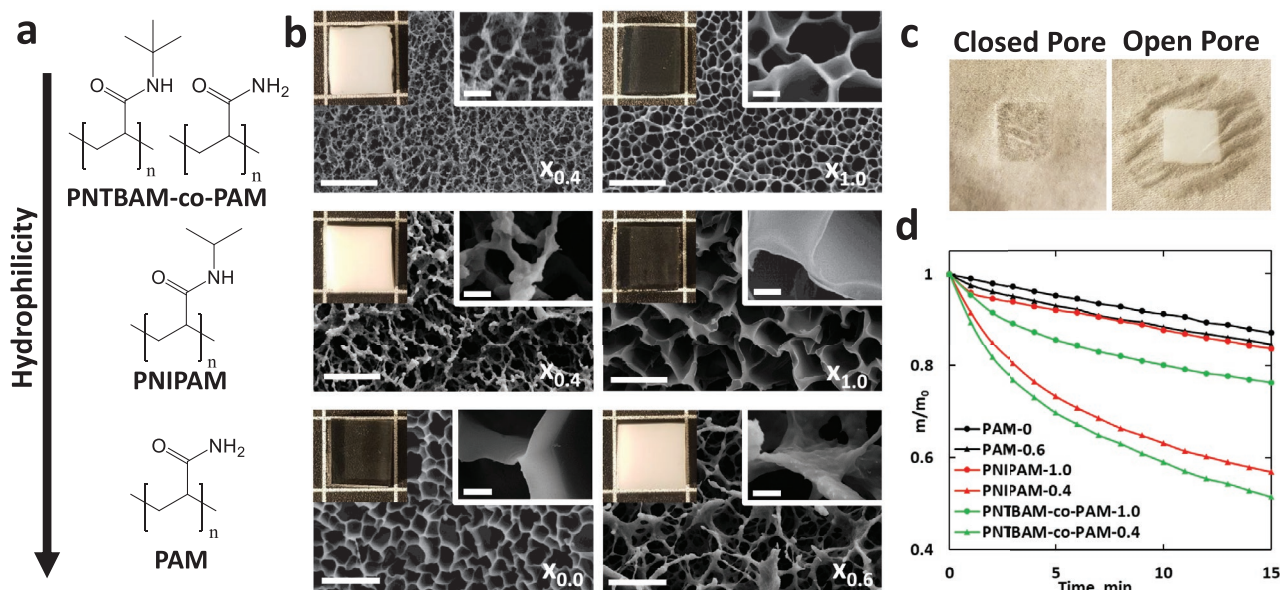


Figure 5. a) Chemical structures of PNTBAM-*co*-PAM, PNIPAM, and PAM in order of increasing hydrophilicity. b) SEM images of PNTBAM-*co*-PAM (top), PNIPAM (middle), and PAM (bottom) hydrogels synthesized at different DMSO mole fractions, demonstrating both open pore and closed pore structures. Inset images depict photographs of the corresponding hydrogels (0.95 cm × 0.95 cm × 3 mm). Scale bars: 10 μm (low mag) and 1 μm (high mag). c) Capillary wicking of water by a tissue after 1 min for $x_{1,0}$ PNIPAM (left) and $x_{0,4}$ PNIPAM (right) hydrogels. d) Mass change over time for closed pore and open pore PNTBAM-*co*-PAM, PNIPAM, and PAM hydrogels during capillary wicking of water.

materials, there remain significant challenges in generalizing this technique to more desirable polymer systems with chemical structures significantly different from PNIPAM. Future studies can greatly benefit from studying this synthetic framework from both fundamental and engineering perspectives to produce novel porous materials for specifically tailored applications in soft robotics, solar vapor generation, energy storage, catalysis, drug release, and biosensing.

Supporting Information

Supporting Information is available from the Wiley Online Library or from the author.

Acknowledgements

Y.A. and S.W. contributed equally to this work. The authors acknowledge the support of ONR award N00014-17-1-2117, ONR award N00014-18-1-2314, AFOSR award FA9550-17-1-0311, AFOSR award FA9550-18-1-0449, AFOSR award FA9550-20-1-0344, NSF CAREER award 1724526, the Hellman Fellows Funds, and start-up funds from the University of California, Los Angeles.

Conflict of Interest

The authors declare no conflict of interest.

Data Availability Statement

The data that support the findings of this study are available from the corresponding author upon reasonable request.

Keywords

3D printing, diffusion, hierarchical structures, hydrogels, stimuli-responsive materials

Received: December 7, 2020

Revised: February 7, 2021

Published online: April 8, 2021

- [1] Q. Shi, H. Liu, D. Tang, Y. Li, X. J. Li, F. Xu, *NPG Asia Mater.* **2019**, *11*, 64.
- [2] X. Zhou, Y. Guo, F. Zhao, G. Yu, *Acc. Chem. Res.* **2019**, *52*, 3244.
- [3] Y. Guo, J. Bae, F. Zhao, G. Yu, *Trends Chem.* **2019**, *1*, 335.
- [4] J. Li, D. J. Mooney, *Nat. Rev. Mater.* **2016**, *1*, 16071.
- [5] F. Hapiot, S. Manuel, E. Monflier, *ACS Catal.* **2013**, *3*, 1006.
- [6] J. Tavakoli, Y. Tang, *Polymers* **2017**, *9*, 364.
- [7] J. Wang, S. Gao, J. Tian, F. Cui, W. Shi, *Water* **2020**, *12*, 692.
- [8] A. Bin Imran, T. Seki, Y. Takeoka, *Polym. J.* **2010**, *42*, 839.
- [9] T. Tanaka, D. J. Fillmore, *J. Chem. Phys.* **1979**, *70*, 1214.
- [10] Z. Liu, Y. Faraj, X. J. Ju, W. Wang, R. Xie, L. Y. Chu, *J. Polym. Sci., Part B: Polym. Phys.* **2018**, *56*, 1306.
- [11] B. Ghanbarian, A. G. Hunt, R. P. Ewing, M. Sahimi, *Soil Sci. Soc. Am. J.* **2013**, *77*, 1461.
- [12] A. Einstein, *Ann. Phys.* **1905**, *322*, 549.
- [13] A. Koponen, M. Kataja, J. Timonen, *Phys. Rev. E: Stat., Nonlinear, Soft Matter Phys.* **1996**, *54*, 406.
- [14] N. Bodenberger, D. Kubiczek, I. Abrosimova, A. Scharm, F. Kipper, P. Walther, F. Rosenau, *Biotechnol. Rep.* **2016**, *12*, 6.
- [15] W. W. Thein-Han, R. D. K. Misra, *Acta Biomater.* **2009**, *5*, 1182.
- [16] T. Serizawa, K. Wakita, M. Akashi, *Macromolecules* **2002**, *35*, 10.
- [17] S. Xue, Y. Wu, J. Wang, M. Guo, D. Liu, W. Lei, *Materials* **2018**, *11*, 1069.
- [18] E. Lee, D. Kim, H. Kim, J. Yoon, *Sci. Rep.* **2015**, *5*, 15124.
- [19] T. Gancheva, N. Virgilio, *Macromolecules* **2016**, *49*, 5866.
- [20] T. V. Chirila, I. J. Constable, G. J. Crawford, S. Vijayasekaran, D. E. Thompson, Y. Chen, W. A. Fletcher, B. J. Griffin, *Biomaterials* **1993**, *14*, 26.
- [21] S. Chang, M. Kim, S. Oh, J. H. Min, D. Kang, C. Han, T. Ahn, W. G. Koh, H. Lee, *Polymer* **2018**, *145*, 174.
- [22] C. Ji, A. Khademhosseini, F. Dehghani, *Biomaterials* **2011**, *32*, 9719.
- [23] R. A. Gemeinhart, H. Park, K. Park, *Polym. Adv. Technol.* **2000**, *11*, 617.
- [24] K. S. Anseth, C. N. Bowman, L. Brannon-Peppas, *Biomaterials* **1996**, *17*, 1647.
- [25] M. Ebner, D. W. Chung, R. E. Garcia, V. Wood, *Adv. Energy Mater.* **2014**, *4*, 1301278.
- [26] B. S. Forney, C. Baguenard, C. A. Guymon, *Soft Matter* **2013**, *9*, 7458.
- [27] S. Deville, *Ice-Templating: Processing Routes, Architectures, and Microstructures*, Springer, Cham, Switzerland **2017**, pp. 171–252.
- [28] S. Sornkamnerd, M. K. Okajima, T. Kaneko, *ACS Omega* **2017**, *2*, 5304.
- [29] Z. Zhang, L. He, C. Zhu, Y. Qian, L. Wen, L. Jiang, *Nat. Commun.* **2020**, *11*, 875.
- [30] E. W. J. Mardles, *J. Soc. Chem. Ind.* **1923**, *42*, 127.
- [31] F. M. Winnik, H. Ringsdorf, J. Venzmer, *Macromolecules* **1990**, *23*, 2415.
- [32] H. G. Schild, M. Muthukumar, D. A. Tirrell, *Macromolecules* **1991**, *24*, 948.
- [33] K. Mukae, M. Sakurai, S. Sawamura, K. Makino, S. W. Kim, I. Ueda, K. Shirahama, *J. Phys. Chem.* **1993**, *97*, 737.
- [34] T. Kanaya, N. Takahashi, H. Takeshita, M. Ohkura, K. Nishida, K. Kaji, *Polym. J.* **2012**, *44*, 83.
- [35] H. Yamauchi, Y. Maeda, *J. Phys. Chem. B* **2007**, *111*, 12964.
- [36] R. O. R. Costa, R. F. S. Freitas, *Polymer* **2002**, *43*, 5879.
- [37] H. Kojima, F. Tanaka, C. Scherzinger, W. Richtering, *J. Polym. Sci., Part B: Polym. Phys.* **2013**, *51*, 1100.
- [38] S. Maccarrone, C. Scherzinger, O. Holderer, P. Lindner, M. Sharp, W. Richtering, D. Richter, *Macromolecules* **2014**, *47*, 5982.
- [39] T. Amiya, Y. Hirokawa, Y. Hirose, Y. Li, T. Tanaka, *J. Chem. Phys.* **1987**, *86*, 2375.
- [40] C. S. Biswas, Q. Wang, B. Du, F. J. Stadler, *Polym. Test.* **2017**, *62*, 177.
- [41] C. S. Biswas, V. K. Patel, N. K. Vishwakarma, A. K. Mishra, B. Ray, *J. Appl. Polym. Sci.* **2011**, *121*, 2422.
- [42] H. Tokuyama, N. Ishihara, S. Sakohara, *Polym. Bull.* **2008**, *61*, 399.
- [43] K. Kyriakos, M. Philipp, J. Adelsberger, S. Jaksch, A. V. Berezkin, D. M. Lugo, W. Richtering, I. Grillo, A. Miasnikova, A. Laschewsky, P. Müller-Buschbaum, C. M. Papadakis, *Macromolecules* **2014**, *47*, 6867.
- [44] I. Bischofberger, D. C. E. Calzolari, P. De Los Rios, I. Jelezarov, V. Trappe, *Sci. Rep.* **2015**, *4*, 4377.
- [45] D. Mukherji, C. M. Marques, K. Kremer, *Nat. Commun.* **2014**, *5*, 4882.
- [46] X. Z. Zhang, Y. Y. Yang, T. S. Chung, *Langmuir* **2002**, *18*, 2538.
- [47] B. G. Kabra, S. H. Gehrke, *Polym. Commun.* **1991**, *32*, 322.
- [48] S. X. Cheng, J. T. Zhang, R. X. Zhuo, *J. Biomed. Mater. Res., Part A* **2003**, *67*, 96.

- [49] X. Z. Zhang, R. X. Zhuo, *Macromol. Chem. Phys.* **1999**, *200*, 2602.
- [50] W. Xue, I. W. Hamley, M. B. Huglin, *Polymer* **2002**, *43*, 5181.
- [51] Y. Kaneko, K. Sakai, A. Kikuchi, R. Yoshida, Y. Sakurai, T. Okano, *Macromolecules* **1995**, *28*, 7717.
- [52] Y. Noguchi, K. Okeyoshi, R. Yoshida, *Macromol. Rapid Commun.* **2005**, *26*, 1913.
- [53] E. S. Gil, S. M. Hudson, *Biomacromolecules* **2007**, *8*, 258.
- [54] C. Mou, X. Ju, L. Zhang, R. Xie, W. Wang, N. Deng, J. Wei, Q. Chen, L. Chu, *Langmuir* **2014**, *30*, 1455.
- [55] L. W. Xia, R. Xie, X. J. Ju, W. Wang, Q. Chen, L. Y. Chu, *Nat. Commun.* **2013**, *4*, 2226.
- [56] X. M. Ma, R. Li, J. Ren, X. C. Lv, X. H. Zhao, Q. Ji, Y. Z. Xia, *RSC Adv.* **2017**, *7*, 47767.
- [57] P. Li, X. Hou, L. Qu, X. Dai, C. Zhang, *Polymers* **2018**, *10*, 137.
- [58] W. J. Zheng, N. An, J. H. Yang, J. Zhou, Y. M. Chen, *ACS Appl. Mater. Interfaces* **2015**, *7*, 1758.
- [59] C. Liu, J. Yu, G. Jiang, X. Liu, Z. Li, G. Gao, F. Liu, *J. Mater. Sci.* **2013**, *48*, 774.